Near-fault anisotropy following the Hector Mine earthquake

Elizabeth S. Cochran and John E. Vidale
Earth and Space Sciences, University of California, Los Angeles, California, USA

Yong-Gang Li
Earth Sciences, University of Southern California, Los Angeles, California, USA

Received 18 December 2002; revised 5 May 2003; accepted 13 June 2003; published 18 September 2003.

[1] We present anisotropy measurements from shear wave splitting along the Hector Mine rupture zone. Six major arrays were deployed in four locations in the year following the M7.1 Hector Mine earthquake. The dense station coverage, wide distribution of the arrays, and repeated deployments show a clear predominant fast direction and spatial variation of splitting along the fault but no resolvable temporal variations. We determined splitting parameters using an automated cross-correlation method, discarding fast directions with initial source polarizations near crack parallel or perpendicular directions. Only two of the four array locations give reliable measurements of anisotropy at depth. Fast directions and delay times are constant across the 1 km wide array length. However, some spatial variation of splitting is observed along fault strike. Delay times decrease from north to south, with greater splitting in areas of higher slip. A change in splitting parameters along fault strike likely reveals the orientation of cracking in the near-fault region during a major quake. Average fast directions are between fault parallel and the regional maximum compressive stress direction. We do not see temporal evolution in anisotropy; however, measured splitting suggests a heterogeneous stress field partially created during rupture that persists over at least a 1 year timescale. *INDEX TERMS:* 7205 Seismology: Continental crust (1242); 7209 Seismology: Earthquake dynamics and mechanics; 8164 Tectonophysics: Stresses—crust and lithosphere; *KEYWORDS:* anisotropy, 1999 Hector Mine earthquake, spatial distribution, stress, shear wave splitting, fault zone

Citation: Cochran, E. S., J. E. Vidale, and Y.-G. Li, Near-fault anisotropy following the Hector Mine earthquake, *J. Geophys. Res.*, *108*(B9), 2436, doi:10.1029/2002JB002352, 2003.

1. Background

[2] Following the 1999 M7.1 Hector Mine earthquake, we deployed several dense seismic arrays across the surface rupture. Shear wave splitting observations were made at the Hector Mine rupture zone in three time windows spanning 1 year. The Hector Mine earthquake provides a natural setting for studying fault properties associated with a large magnitude event. The accessibility of the rupture allowed a unique opportunity to deploy numerous instruments immediately following the main shock and redeployment in subsequent years. The clear surface break and near-vertical fault rupture also facilitates comparison of on- and off-fault anisotropy.

[3] Crustal anisotropy as determined by shear wave splitting is most likely the result of aligned microcracks referred to as extensive dilatancy anisotropy (EDA) [*Crampin*, 1978]. This model has since been modified leading to the anisotropic poroelasticity model (APE) [*Crampin and Zatsepin*, 1997; *Zatsepin and Crampin*, 1997]. *Nur and Simmons* [1969] showed experimentally that cracks open parallel to the minimum compressive stress and are aligned parallel to the maximum compressive stress direction (σ_h). Thus, vertical cracks in a strike-slip regime tend to align parallel to σ_h. Splitting parameters determined near faults can therefore reveal stresses acting on the fault, assuming no other causes of anisotropy. Temporal variations of fine-scale anisotropy orientations or amplitude have been taken to indicate healing along the fault or changes in relative stress amplitudes [*Crampin*, 1987].

[4] A better understanding of fault structure provides information on mechanical properties of faulting. Fault - geometry and orientation, slip rates, lithology, temperature, and pore pressure are all faulting mechanical properties that control rupture initiation, propagation, and cessation [*Li et al.*, 1999]. EDA cracks may also modulate high pore fluid pressures necessary for movement on a fault [*Crampin*, 1987].

[5] Studies of shear wave anisotropy have been numerous in the past several years and some may indicate that anisotropy varies with fault locality and activity. Previous studies have claimed spatial and temporal variations at active fault zones. Several studies show a rotation of fast direction measured near active faults to near fault parallel. For paths outside active faults and near less recently active faults crustal anisotropy measurements show fast directions parallel to σ_h [e.g., *Zhang and Schwartz*, 1994; *Zinke and*

0148-0227/03/2002JB002352$09.00

Zoback, 2000]. Temporal variations of shear wave splitting have been observed in some studies following large earthquakes or swarms [e.g., *Booth et al.*, 1990; *Gao et al.*, 1998; *Tadokoro and Ando*, 2002].

[6] However, many of the studies use data from only one or two instruments near a fault zone to draw conclusions about spatial and temporal patterns of stress near the fault. Some studies observe no change in anisotropy even in the presence of stress perturbing events [e.g., *Aster et al.*, 1990; *Munson et al.*, 1995]. For a better resolved picture of anisotropy along an active fault, we examine data from arrays of seismometers deployed in several locations along the main surface rupture of the Hector Mine earthquake. Using closely spaced stations, we can investigate the spatial extent of anisotropy across the narrow fault zone. In addition, instruments deployed in linear arrays crossing the fault allow for noise suppression by stacking.

[7] Trapped wave studies indicate healing occurs within a 100–200 m wide fault zone following a main shock rupture. In several studies of P and S velocities along the Landers and Hector Mine rupture zone, a 1% increase in wave speed has been observed on a 1 year timescale following the main shock [*Li et al.*, 2002; *Vidale and Li*, 2003]. Our study of anisotropy examines whether changes in crack orientation or density can be observed to constrain the depth extent and material change responsible for the observed velocity increase.

2. Hector Mine Main Shock

[8] The M7.1 Hector Mine earthquake occurred on 16 October 1999 at 2:46am, within the Mojave block of the eastern California shear zone. The main shock ruptured two faults: the Bullion fault and the previously unnamed Lavic Lake fault. The rupture was bilateral, with approximately 10 km of surface rupture to the north and 33 km to the south (Figure 1).

[9] To the north, the earthquake ruptured two fault segments, although surface rupture in this area was limited to the western segment, which strikes N45°W. The eastern segment did not rupture to the surface, but is clearly delineated by aftershock locations and strikes roughly north-south. Large surface slips up to 5.2 m were confined to the northern end of the rupture [*Treiman et al.*, 2002]. The central portion of the fault strikes N10°W and is a fairly simple, linear fault. Along the southern end of the rupture the fault again bifurcates. Total slip is much lower and distributed on several fault splays striking roughly N35°W. Average total surface slip during the Hector Mine main shock was approximately 3 m.

3. Field Methods

[10] To determine a suite of splitting directions, we examine data from each seismic array deployed after the main shock. Three main deployments took place in the days, months, and years following the main shock (Figure 1).

[11] A dense Geometrics array (GEOM99) was deployed days after the Hector Mine earthquake, 24–30 October 1999, approximately 5 km south of the main shock epicenter. The line had 20 stations with 5 m spacing, spanning 100 m across the fault. The surface slip observed at the array location was 5 m and was concentrated on a few closely spaced splays within the array.

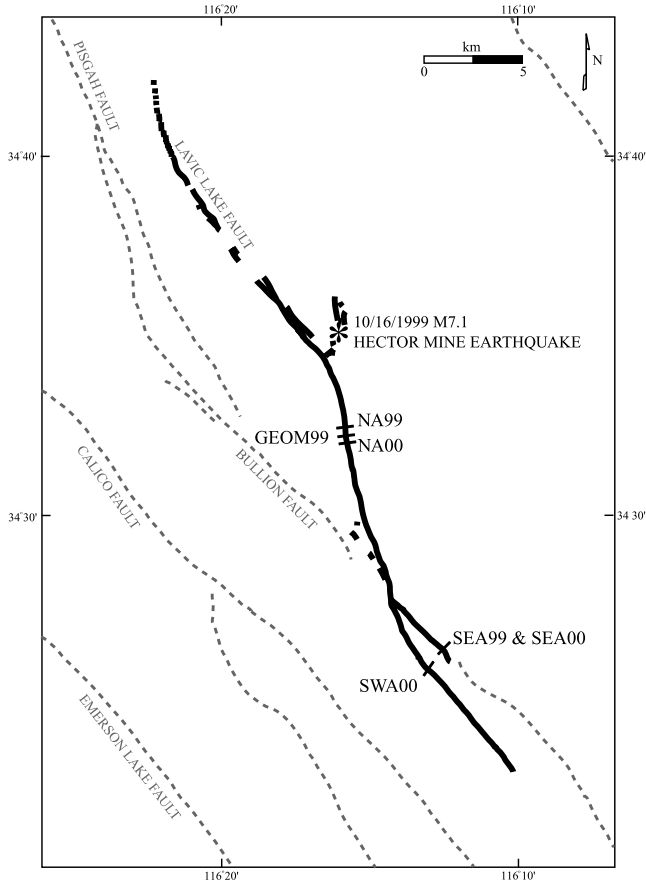

Figure 1. Regional map indicating surface rupture (solid black) of the Hector Mine (M7.1) earthquake (epicenter indicated by star). Regional faults are shown by the dashed grey lines. Labeled bars crossing the surface rupture indicate 1999 and 2000 array locations.

[12] A larger deployment took place 31 October to 30 November 1999 consisting of two main seismic arrays. The arrays used a portable deployment of REFTEK systems with L22 sensors. The northern array (NA) was located in the Bullion Mountains 5 km south of the main shock, in the vicinity of the earlier Geometrics deployment. The array had several components: a line of ten stations along the fault trace spanning 2 km and a line of twenty stations perpendicular to the fault trace in a cross-fault array with irregular station spacing (12.5–100 m) spanning 1 km. The southeastern array (SEA) was located in Bullion Wash on one strand of the fault bifurcation, 15 km south of the main shock. The array had over 50 seismic stations. Again, stations were deployed in along- and cross-fault arrays. An additional component of SEA was a two-dimensional grid of 25 instruments at a station spacing of 50 m deployed on the eastern side of the fault trace.

[13] A more recent deployment took place 9 September to 23 October 2000. NA00 was relocated 1 km south of the 1999 site for easier access. SEA00 was redeployed at the same location. An additional array (SWA) was deployed on a fault splay 2 km west of the southeastern array site. Each of these arrays had a line of 21 stations crossing the fault with irregular

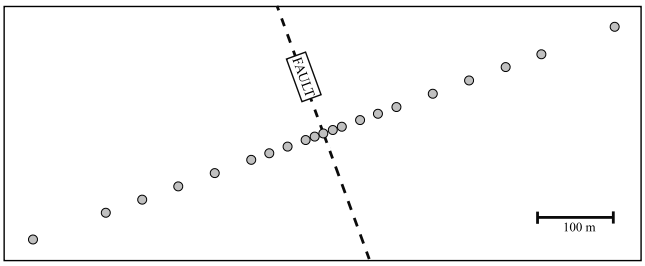

Figure 2. Diagram of cross-fault array layout. Fault location is indicated by dashed line. Station spacing is 12.5 m near the fault increasing to 100 m away from the fault.

spacing (12.5 to 100 m) spanning 1 km (Figure 2). The spacing was densest across the fault trace.

[14] Owing to the remote location of the rupture, ideal field conditions allowed recording of high-quality seismograms with low ambient noise. Each deployment recorded thousands of aftershocks. In this study, we use only double-difference relocated catalog events to ensure accurate locations (E. Hauksson, personal communication, 2001).

4. Methodology

[15] Anisotropy is observed when a seismic wave travels through a medium that contains aligned minerals or cracks. In the upper crust, anisotropy is most often caused by parallel fluid-filled cracks [*Crampin*, 1978]. As a shear wave travels through an anisotropic medium, the wave is split into two quasi-shear waves: one polarized parallel and one polarized perpendicular to the cracks (Figure 3). The quasi-shear wave polarized parallel to the cracks travels at a higher velocity and thus arrives at a seismic station first. We examine the orientation and density of cracks around the Hector Mine rupture to study stress near a fault, rupture mechanics, and temporal evolution of a fault zone.

[16] The cross-correlation method was used to determine shear wave splitting parameters [e.g., *Zhang and Schwartz*, 1994]. A search is performed on horizontal traces windowed around the S arrival over all angles, by one degree increments, and delay times, from −0.2 to 0.2s, to determine the maximum cross-correlation between horizontal components. The cross-correlation value is a measure of the similarity of pulse shape for the two horizontal components and is independent of relative or absolute amplitude. The angle and time lag with the maximum cross-correlation value corresponds to the orientation of the fast arriving shear wave and delay time between the fast and slow arriving polarizations.

[17] Only catalog events within the shear wave window are examined for splitting parameters. Events within the shear wave window have an angle of incidence of 35 degrees or less and thus are less likely to be contaminated by near-critical S to P conversions near the surface [*Booth and Crampin*, 1985; *Nuttli*, 1961]. In this study, events with a straight ray path incidence of 45 degrees or less are used, assuming incident waves turn toward vertical as they travel through low velocity sediments near the surface.

[18] To ensure data quality, we used only events triggered by at least ten cross-fault array stations. Seismograms are low-pass filtered at 15 Hz to remove noise. The applied filter does not degrade the results as the S-waves have a dominant frequency of about 5–8 Hz. All traces are normalized, and then stacked on hand-picked S-wave arrivals (Figure 4). Splitting parameters measured for the cross-fault array stack are compared with those measured for both individual stations and smaller stacks. No significant changes in orientation or delay time are seen for individual stations when compared with entire array stacks. Therefore splitting is caused by pervasive anisotropy of at least the same length scale as the array. Stacking improves the signal-to-noise ratio, allowing for a more stable estimate of splitting parameters. Stacked traces give higher correlation values with stable splitting parameters over various windows around the S-arrival.

[19] If appropriately determined, splitting parameters can be used to "correct" the wave back to its initial linear source polarization. One measure of the accuracy of splitting parameters is to show that elliptically polarized S-wave arrivals can be corrected back to a linear arrival (Figure 5). A more automatic check of the stability of the cross-correlation method was employed such that two 0.40s time windows are chosen around the S-wave arrival. These windows are shifted by 0.05s and cross-correlation method employed on both time windows to determine whether splitting parameters are stable over the two time windows. Fast directions and delay times that are not within 30 degrees and 20 ms, respectively, are discarded. Cycle skipping is a concern in using the cross-correlation method, and we use these two time windows to minimize this contamination. Only splitting parameters with cross-correlation values of 0.70 or greater are presented.

5. Results

5.1. Overall

[20] Splitting results for each array are shown in Figure 6. Splitting parameters measured along the fault are scattered,

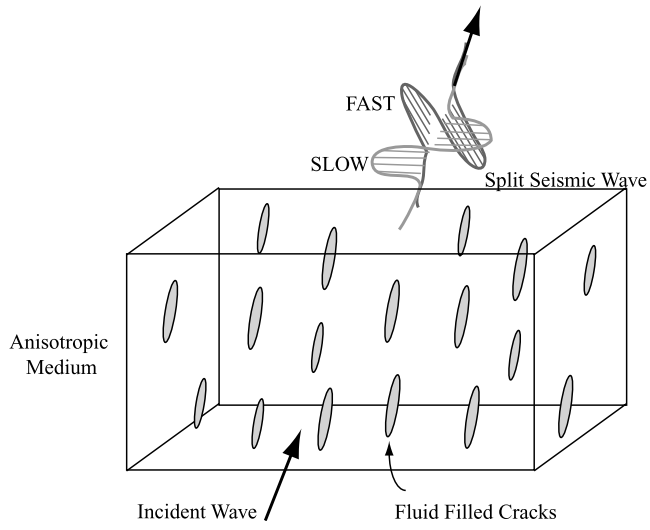

Figure 3. Schematic representation of split shear waves after traveling through an anisotropic medium containing aligned vertical microcracks. Microcracks are assumed to open parallel to the minimum compressive horizontal stress and are aligned parallel to the direction of maximum compressive stress. Splitting observed at seismic station reflects crack orientation and density along the path between the source and receiver.

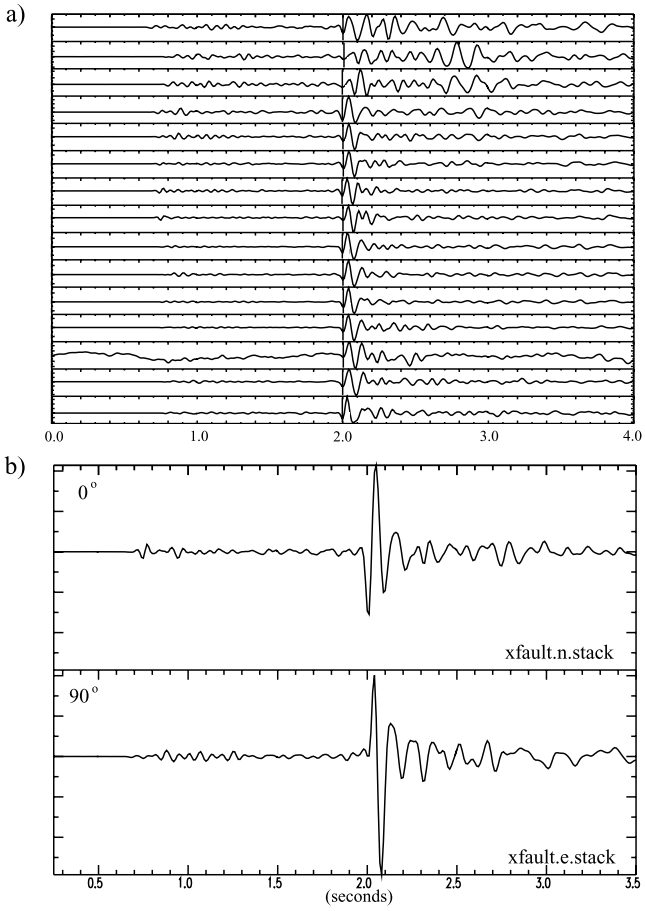

Figure 4. Example of stacking horizontal traces on S-wave arrival. (a) Cross-fault station traces of the east-west component recorded on array SEA00. Vertical lines indicate S picks. (b) Stacked traces; upper trace shows the stacked NS component and lower trace shows the EW stack.

but suggest both general agreement and spatial patterns. Fast directions range from fault-parallel to fault-perpendicular. However, in general, the fast orientation is 0° to 60° east of fault strike.

[21] The Geometrics array (GEOM99) deployed one week following the main shock recorded 37 aftershocks with reliable splitting results. Both fast orientations and delay times are scattered: orientations range from fault-parallel to fault-perpendicular and delay times range from 0 ms to >100 ms. The GEOM99 stations were concentrated along a 100 m line crossing the fault and therefore lack the spatial averaging of the other arrays.

[22] In 1999, the 60 aftershocks for the northern array (NA99) show splitting results with fairly consistent fast directions, but some scatter in delay times. Delay times average about 30 ms but some events have small splitting times of 10 ms or less. In addition, fast directions for several events close to the fault rotate toward fault parallel; however, this result is not statistically significant.

[23] The splitting parameters measured for 73 events recorded on the southeastern array (SEA99) show some scatter in fast direction and delay times. The majority of fast directions are oriented roughly north-south. In addition, delay times tend to decrease toward the southern part of the rupture.

[24] The three arrays deployed in 2000 recorded fewer aftershocks due to a significant decrease in seismicity rate. Splitting parameters for the northern array (NA00) and southeastern array (SEA00), with 28 and 32 events, respectively, show fairly consistent fast directions and delay times. Qualitatively, splitting parameters are less scattered than the 1999 results.

[25] At the southwestern array (SWA00) measured anisotropy is bimodal. Roughly 70% of splitting parameters have a fast direction of 90° and delay time of 20 ms or less (Figure 6d). The remaining 30% of the splitting measurements are orientated near N45°E with delay times of roughly 100 ms. We infer that anisotropy measured at this array is being modified by low-velocity structure near the surface. Shear wave arrivals can be distorted at the free surface due to refraction across near-surface interfaces between rock and sediment [*Crampin*, 1990]. P- and S-wave velocities measured at this site are significantly lower than those measured at the nearby SEA site only 2 km away; 5.1 km/s versus 4.8 km/s; 3.0 km/s versus 2.6 km/s, respectively.

[26] In later plots, data from Geom99 and SWA00 will be discarded leaving the two arrays deployed in both 1999 and 2000: NA and SEA. This selection is done to focus on coherent spatial and temporal variation of anisotropy at depth. We will not discuss Geom99 and SWA00 further; however, they may contain subtleties of the fault zone that may be pursued in the future. Namely, Geom99 may show more extreme variation due to a stronger cracking at the earliest time after the main shock and SWA00 may reveal interesting near-surface structure.

5.2. Initial Polarization

[27] One limitation inherent to shear wave splitting analysis is certain shear wave source polarizations will be unable to resolve anisotropy. If the source polarization of an earthquake is nearly parallel or perpendicular to crack orientation, the shear wave will not be split into a fast and slow polarization [*Leary et al.*, 1990]. Therefore these events do not sample the main anisotropic field and should be discarded. We plot splitting parameters versus initial source polarization in Figure 7 for NA and SEA. Initial source polarizations are determined from seismograms as focal mechanisms are not available for the aftershocks. Events with initial shear wave polarizations close to north-south or east-west show anomalous fast directions and delay times. Therefore the main crack field is probably oriented close to one of these two directions. We discard 40 events with initial polarizations within ±10° of the inferred fast or slow directions shown in the shaded region of Figure 7.

5.3. Error Analysis

[28] For a more quantitative analysis of the data we determine averages of both fast directions and delay times. Averaging delay times is trivial and we present the mean delay time and associated standard error. However, directional data requires more detailed statistical analysis. Fast orientations have 180 degree symmetry and must be treated as axial data. Therefore we double the angles before applying any statistical methods. To determine variance

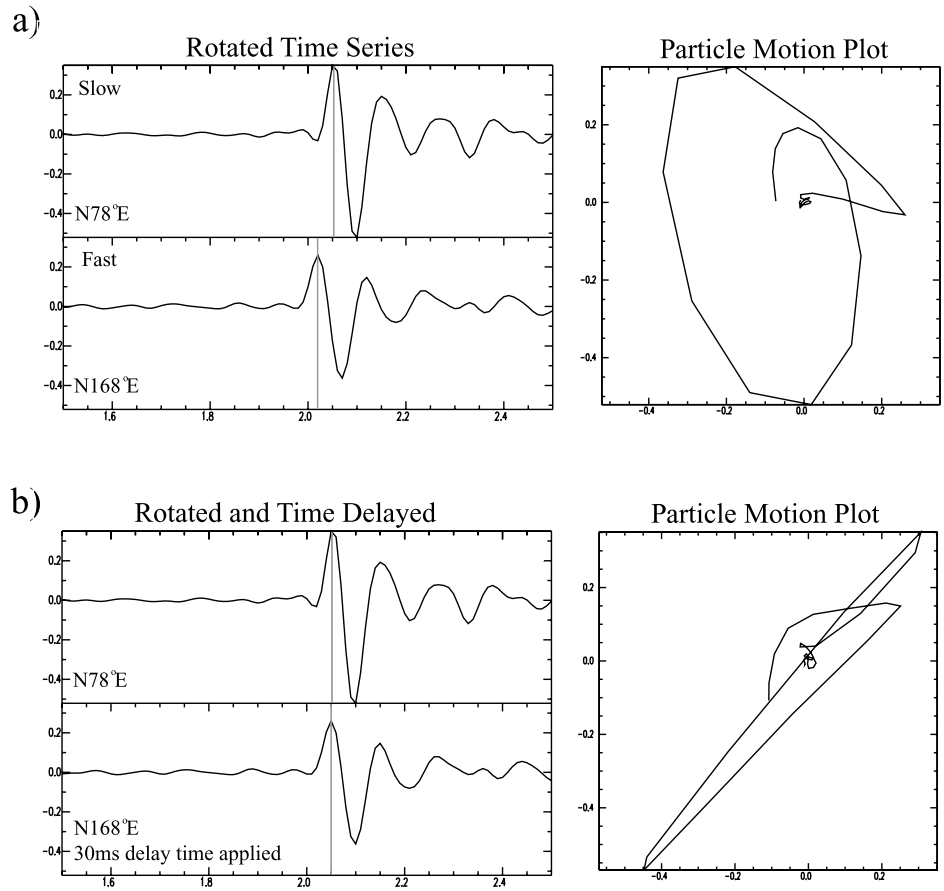

Figure 5. Example of the cross-correlation method for one event. (a) Traces rotated to the slow (upper trace) and fast (lower trace) orientation. Note that S-wave arrival comes in several 10s of ms sooner on the lower trace than the upper trace. On the right, the particle motion for the split shear wave is plotted showing obvious elliptical motion. (b) A delay time of 30 ms has been applied to the fast component (lower trace) to align the two shear wave arrivals. The particle motion plot now shows the expected linear arrival of an "unsplit" shear wave.

and standard errors for directional data we use the von Mises method [*Davis*, 1986; *Mardia and Jupp*, 2000]. This method assumes a normal distribution of circular data much like what is used for linear normal distributions. We calculate the mean angle $\theta = \tan^{-1}\left[(\Sigma_{i=1}^{n} \sin\theta_i)/(\Sigma_{i=1}^{n} \cos\theta_i)\right]$ and a mean resultant length $R = \sqrt{\left[(\Sigma_{i=1}^{n} \sin\theta_i)^2 + (\Sigma_{i=1}^{n} \cos\theta_i)^2\right]}$ which is a measure of the variance. The mean resultant length varies between 0 and 1, with values near 1 indicating high clustering of the data. In addition we can compute a standard error using the formula $1/\sqrt{(\kappa\, n\, R)}$ where n is the number of samples and κ is the maximum likelihood estimate of the concentration parameter from *Davis* [1986]. Fast directions are presented using rose diagrams showing a circular histogram of the axial data. In addition, we have plotted on the rose diagram a vector oriented in the mean direction (θ) with length proportional to the mean resultant length (R).

5.4. Binning

[29] The weighted average of all 153 splitting measurements determined for NA and SEA indicates a fast direction of N3°E ± 4° and delay of 32 ± 2 ms. Figure 8 compares splitting parameters measured at NA and SEA in 1999 and 2000. Events with initial source polarizations near the fast or slow direction have been discarded as indicated above.

[30] We present average splitting parameters in two ways. First, the results are averaged by array and year. Table 1 and Figure 9 give the averages for NA99, SEA99, NA00, and SEA00. The averages may indicate a slight rotation along fault strike and between 1999 and 2000, but these results are not statistically significant. Delay times remain roughly constant for all four data sets.

[31] Second, the study area is divided into three bins at major changes in strike along the fault. Bin 1 covers the northernmost portion of the rupture where the fault is bifurcated into two branches: a buried strand striking roughly NS and a branch that ruptures to the surface striking N45°W. Bin 2 contains the central portion of the surface rupture striking N10°W, with most of the slip concentrated on a single strand. Bin 3 covers the southern end of the rupture, in an area of little slip distributed across several fault strands striking roughly N35°W.

[32] Table 2 presents splitting results for each bin, separated by year. A gradient in average delay time along strike is evident for each of the two years. Delay times decrease along strike from north to south in both the 1999 and 2000

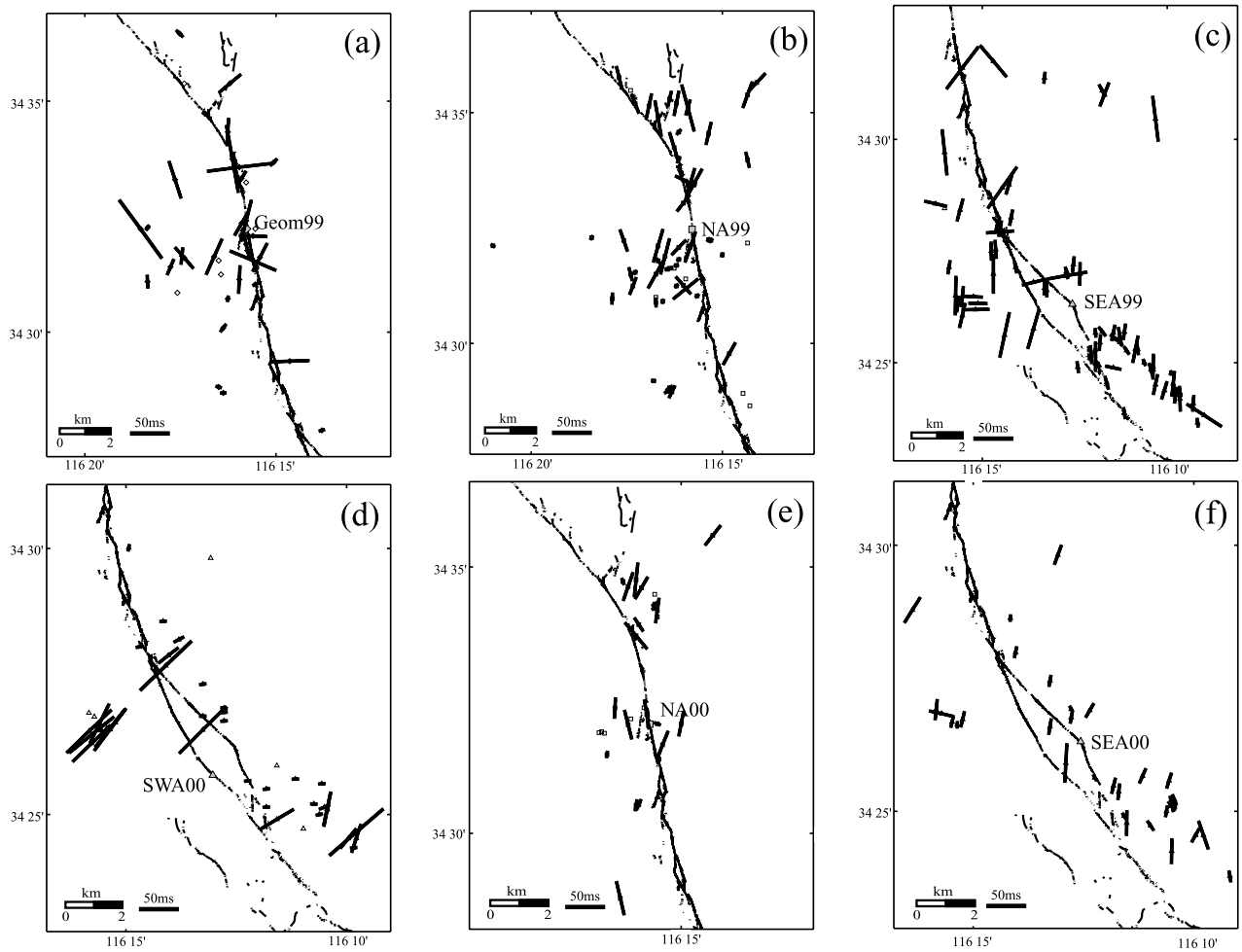

Figure 6. Splitting results for each array deployment: (a) GEOM99, (b) NA99, (c) SEA99, (d) SWA00, (e) NA00, and (f) SEA00. Bars are oriented parallel to the fast direction and are scaled by delay time. Splitting parameters are plotted at the source epicenter.

data sets: 44 ms to 32 ms and 48 ms to 29 ms, respectively. Associated standard errors in the delay times suggest this spatial pattern in delay time is statistically significant. However, there is no observable temporal change in delay times measured for any of the bins over the 1 year study period.

[33] The data suggest some rotation both spatially and temporally. Bins 1 and 3 have fast directions oriented roughly N3°W in 1999, which rotate east to approximately N10°E in 2000. Bin 2 shows an opposite sense of rotation, from N20°E in 1999 to N2°E 1 year later. However, standard error bounds overlap, so neither the spatial nor temporal changes in crack orientation are statistically distinct.

[34] Neither fast direction nor delay time suggest strong temporal changes over the year following the Hector Mine main shock. While there is some indication of temporal rotation of fast direction in bins 1 and 2, the standard error in the averages overlap. In addition, sense of rotation is opposite and does not suggest a consistent trend. Measured delays suggest no temporal evolution of the crack field. Table 3 and Figure 10 give average splitting parameters for each bin, not separated by year. Using these averages we can examine in more detail the spatial characteristics of the crack field.

[35] Bin 1 has an average fast direction of 3° ± 12° and delay time of 45 ± 7 ms. This bin contains the bifurcated northern portion of the rupture with high coseismic slips. The maximum slip at depth is estimated by *Ji et al.* [2002] using a combined inversion of GPS, teleseismic, strong motion, and surface rupture data. In bin 1 the maximum slip is 700 cm on the fault strand oriented at N45W and 500 cm on the NS strand on which the hypocenter was located.

[36] Bin 2 has greater scatter in crack orientation with an average fast direction of 12° ± 8° and corresponding mean resultant length of 0.58. This is surprising as this bin contains the simplest portion of the rupture with most of the slip concentrated on a single strand. However, the events included in this bin are scattered at wider distances from the fault and may encounter a more varied anisotropic field. Delay times measured for this bin are 32 ± 3 ms, much lower than those measured in bin 1. Maximum coseismic slip at depth in this bin ranges from 700 cm to 400 cm, decreasing from north to south.

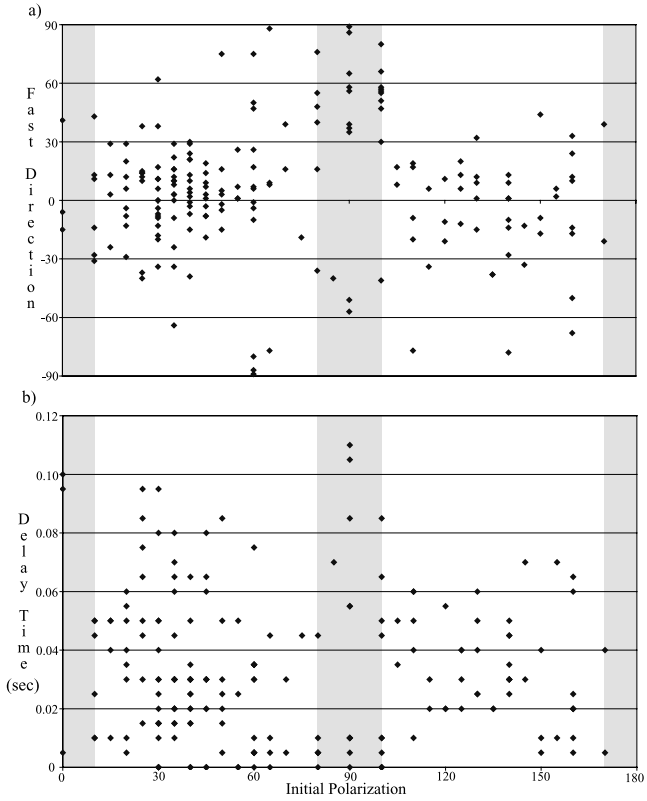

Figure 7. Plot of initial polarization versus (a) fast direction and (b) delay time. Shading indicates areas of anomalous fast directions and delay times, inferred to be parallel or perpendicular to crack orientations.

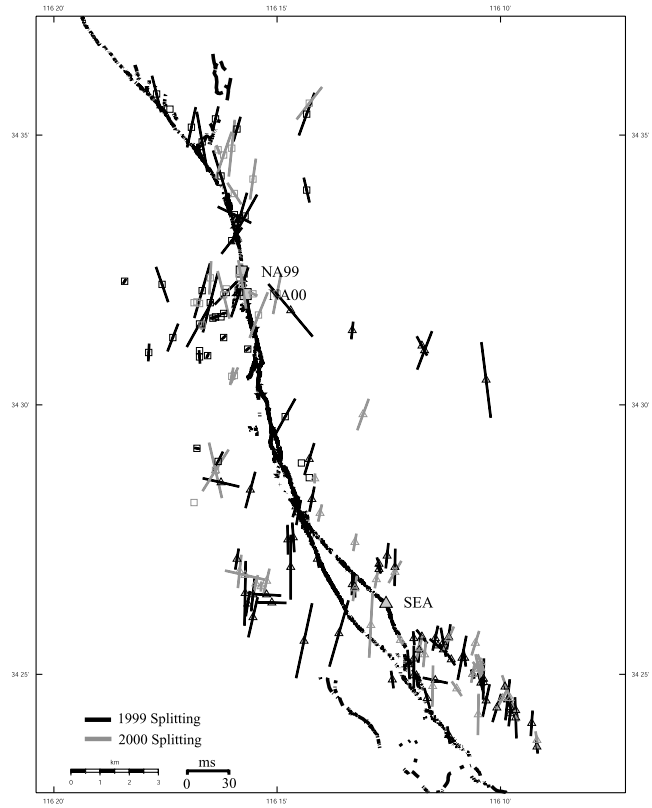

Figure 8. Comparison of splitting results from 1999 and 2000 northern array (NA) and southeastern array (SEA). Bars are oriented parallel to the fast direction and are scaled by delay time. Splitting parameters are plotted at the source epicenter.

[37] Bin 3, containing 82 events, suggests very consistent fast orientations of $-2° \pm 5°$ and delay times of 31 ± 2 ms. This southernmost bin is in an area of low slip spread across several fault strands. Maximum coseismic slips are less than 350 cm, decreasing to essentially zero to the south.

[38] Figure 11 illustrates crack rotation along the fault in relation to Hector Mine rupture strike, regional maximum compressive horizontal stress direction (σ_h), and regional fault strike. It is evident that measured crack orientation is controlled by the recent rupture and σ_h. Regional σ_h was determined by *Hauksson et al.* [2002] using focal mechanisms of pre–main shock events. The fast direction roughly splits the difference between fault strike and regional σ_h, such that crack orientations are rotated $5°-45°$ east of the Hector Mine rupture strike.

5.5. Depth Extent of Anisotropy

[39] Owing to the scatter inherent in delay times determined by shear wave splitting, it is often difficult to constrain the depth extent of anisotropy [e.g., *Gamar and Bernard*, 1997; *Savage et al.*, 1989; *Zhang and Schwartz*, 1994]. Figure 12 plots delay time versus hypocentral distance and versus depth for the 1999 and 2000 NA and SEA arrays. There is not a clear increase in delays with distance or depth. Lacking significant depth dependence, we infer most of the splitting occurs in the upper 2–3 km. Apparent crack density can be estimated from $\varepsilon = \upsilon_s(\delta t/L)$, where ε is the apparent crack density, υ_s is the shear velocity in the uncracked medium and $\delta t/L$ is the path-normalized delay time [*Hudson*, 1981; *O'Connell and Budiansky*, 1974]. We can estimate crack density from the shallowest event with a delay time of 40 ms and hypocentral distance of 2.2 km. For this event, we estimate an apparent crack density of 5% assuming constant crack density along the path. Crack densities may be larger than this estimate if the anisotropic layer is confined to layers less than 2 km thick. However, we see similar splitting at both NA and SEA, which are separated by 10 km, indicating the regional extent of the anisotropic media.

6. Cause and Extent of Anisotropy

[40] A few potential explanations for crustal anisotropy can be invoked to explain shear wave splitting. Foliation, bedding, or aligned minerals are possible alternate explanations to stress induced anisotropy [*Aster and Shearer*, 1992]. However, in the Hector Mine rupture area it is

Table 1. Averaging by Array

	Number of Events	θ°	Δt, ms
NA99	38	19 ± 11	32 ± 4
NA00	22	2 ± 8	30 ± 6
SEA99	63	−4 ± 6	34 ± 3
SEA00	30	3 ± 8	31 ± 3

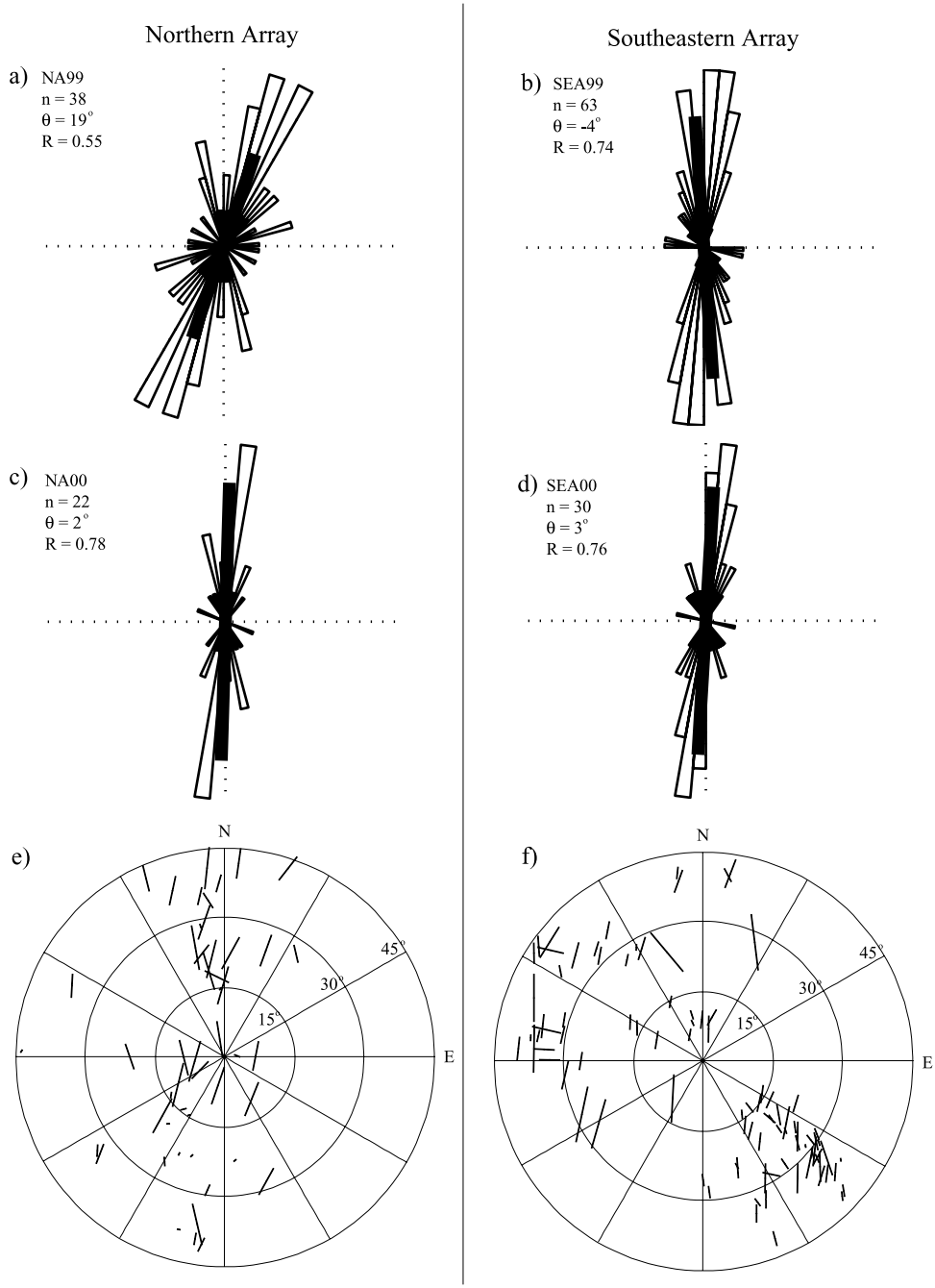

Figure 9. Rose diagrams and equal area plots of fast orientations for each array. Rose diagrams for arrays (a) NA99, (b) SEA99, (c) NA00, and (d) SEA00. Solid black bar indicates average orientation (è) and length of the bar is scaled by the mean resultant length (R). R is a measure of how clustered the data are with larger R indicating greater clustering. n indicates the number of events. (e) Northern array and (f) southeastern array equal area plots of measured splitting parameters. Bars are oriented parallel to the fast direction and are scaled by delay time. Note the straight line angle of incidence spans 0°–45° as we use only events within the shear wave window.

Table 2. Average by Bin: 1999 and 2000

	Number of Events	θ°	Δt, ms
Bin 1 1999	8	−2 ± 14	44 ± 8
Bin 1 2000	4	11 ± 21	48 ± 11
Bin 2 1999	39	20 ± 12	33 ± 4
Bin 2 2000	20	2 ± 9	30 ± 6
Bin 3 1999	54	−4 ± 6	32 ± 3
Bin 3 2000	28	2 ± 8	29 ± 3

Table 3. Average by Bin

	Number of Events	θ°	Δt, ms
Bin 1	12	3 ± 12	45 ± 7
Bin 2	59	12 ± 8	32 ± 3
Bin 3	82	−2 ± 5	31 ± 2

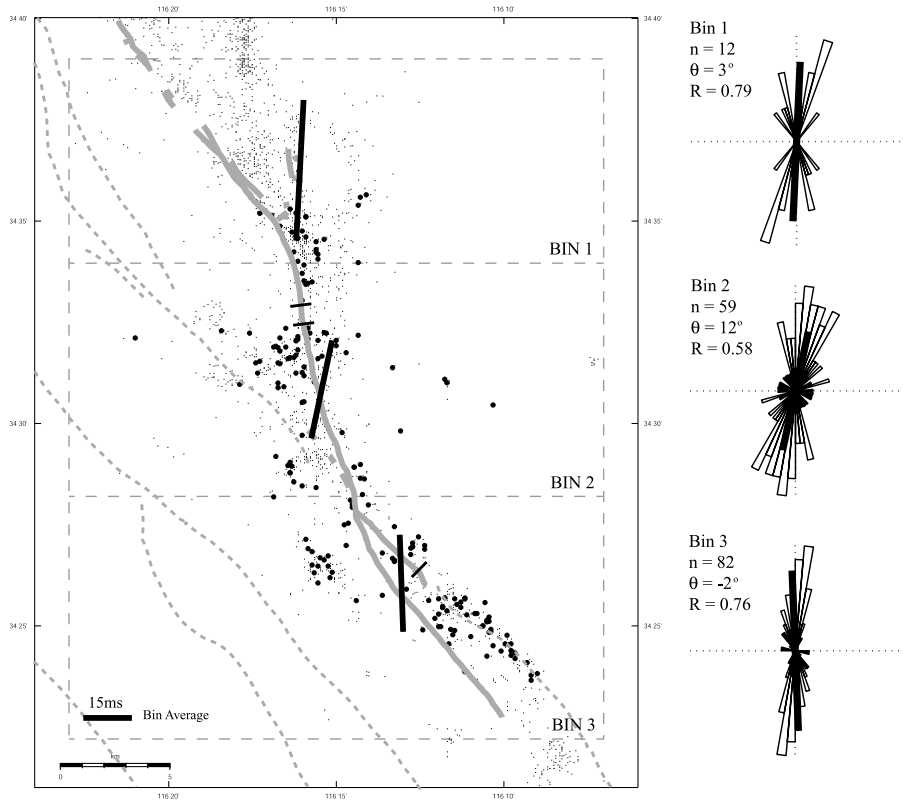

Figure 10. Splitting results binned along fault strike. Bins are chosen based on changes in fault orientation and maximum slip. Bin 1 contains two fault strands with 700 cm of slip on N45W striking fault and 550 cm of slip on the buried fault on which the hypocenter was located. Bin 2 contains a single fault strand with slip decreasing from 700 cm in the north to 400 cm in the south. Bin 3 contains several fault strand with total slip of less than 350 cm. Maximum slip estimates are from *Ji et al.* [2002]. On the left solid black bars indicate average splitting results and are plotted on the rupture map. Bars are oriented in the average fast direction and are scaled by delay time. Note the decrease in delay time from north to south and rotation of fast direction along fault strike. Solid grey line indicates surface rupture during the Hector Mine earthquake, dashed lines give regional fault locations, solid dots indicate events used to determine anisotropy. On the right rose diagrams of the fast direction are plotted with solid black line indicating average fast direction (see Figure 9 for detailed explanation).

unlikely the anisotropy we see is caused by lithologic properties. Our observations suggest anisotropy is pervasive throughout the upper few kilometers as we observe similar anisotropy at both arrays separated by 10 km. Near-surface geology underlying these arrays is quite different with NA located within the Bullion Mountains on a hard rock site and SEA located on the edge of Bullion Wash, a sediment basin. It is difficult to imagine that lithologic properties could cause consistent anisotropy at two arrays when they are underlain by such different material.

[41] We instead invoke EDA, where cracks open in response to the local stress field set up by the Hector Mine earthquake. EDA is suggested by fast orientations measured between fault parallel and regional σ_h. Cracks respond rapidly to changes in the stress field and are likely to be perturbed by a local large magnitude earthquake.

[42] It is difficult to accurately constrain the exact spatial extent of the anisotropic medium. While we resolve average orientations of anisotropy with low standard errors, individual measurements are not well constrained. We cannot therefore evaluate individual measurements for pockets of

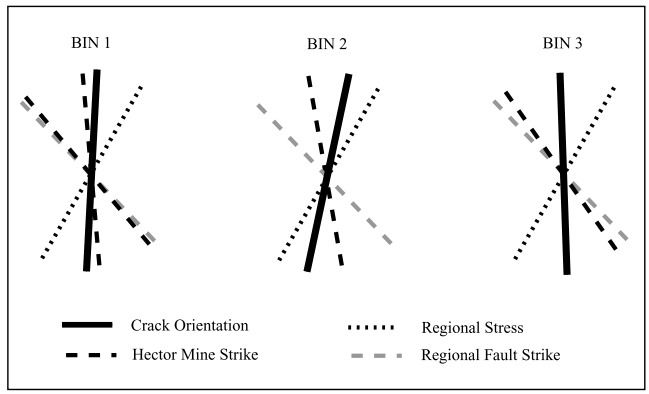

Figure 11. Schematic diagram comparing average crack orientation (solid black) with Hector Mine rupture strike (dashed black), regional maximum compressive stress (dotted), and regional fault strike (dashed grey) for each bin. Fast directions are roughly midway between the Hector Mine rupture strike and regional maximum compressive stress direction (σ_h). Crack orientations are independent of regional fault strike.

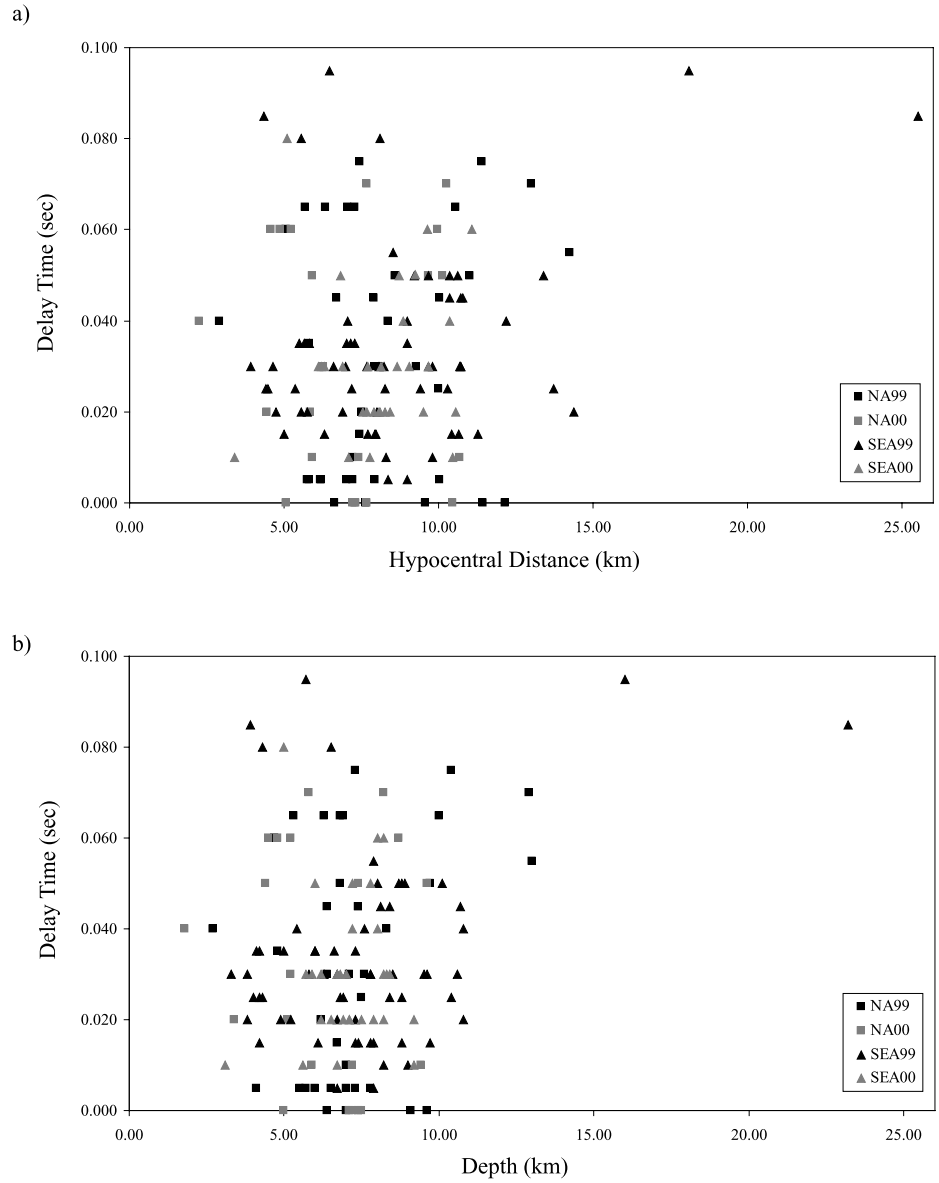

Figure 12. (a) Delay time versus hypocentral distance and (b) delay time versus depth. No systematic changes are observed with distance or depth indicating anisotropy is concentrated in the upper 2–3 km, above the shallowest event.

distinct anisotropy. We can use the data to gain a general sense of where shear wave splitting occurs. On average, no clear increase in anisotropy with depth exists; suggesting cracks are concentrated in the near surface, within the upper 2–3 km. However, anisotropy is constant across the 1 km length of our array. A regional extent to anisotropy is also suggested by consistent splitting at both NA and SEA, separated by 10 km.

[43] We compare our anisotropy results with other studies of the rupture zone at Hector Mine. *Fialko et al.* [2002] examined INSAR data from the Hector Mine rupture region and found 2 km-wide zones near regional faults with reduced elastic modulii that flex with static stress loading. They indicate that fault zones are distinct from surrounding crustal rocks and that these zones may be dynamically weakened. This anomalous compliance is consistent with our observations that cracks opened in response to rupture during the Hector Mine earthquake. Splitting may be confined to these 2 km wide zones; however, lacking better constraints on the spatial extent of anisotropy we are unable to establish this conclusively.

[44] Splitting parameters are not observed to change on a 1 year timescale indicating little postseismic response in crack orientations or densities. *Vidale and Li* [2003] show an increase in P and S velocities following the rupture during 2000–2001 within a narrow 100–200 m wide zone across the fault. They attribute the velocity increase to healing of the fault by closure of cracks. We do not see significant change in average splitting parameters from 1999 to 2000. This may reflect the fact that splitting parameters reflect anisotropy of the entire path that the wave travels, from the source to the receiver. For most

events the path within the narrow fault zone is very short. Our results are regional in nature and do not reflect, primarily, properties of the fault zone. In addition, *Vidale and Li* [2003] observed only a 1–2% increase in P and S wave velocities, an effect that may be too small to observe with shear wave splitting.

7. Conclusions

[45] Anisotropy measured along the Hector Mine fault zone suggests that cracks opened at least partially in response to the main shock rupture. No statistically significant temporal variations are observed in either orientation or delay times over the 1 year following the Hector Mine main shock. However, along strike we see rotation of the fast direction and a statistically significant decrease in delay times from north to south. Average fast directions are oriented between N2°W to N12°E, roughly midway between fault strike and the regional stress direction (σ_h). We may be seeing nearly equal contribution to the crack field from fault fabric and regional σ_h. Delay times decrease from 45 ± 7 ms in bin 1 to 31 ± 2 ms in bin 3. The significantly decrease from north to south correlates with areas of high slip. Therefore areas of higher slip have a higher density of EDA cracks. This may indicate localized weakening of an area during high slip. The spatial extent of anisotropy is difficult to constrain due to scatter in measured delay times. We do not see significant depth dependence on measured delay times, so we infer most of the splitting occurs in the upper 2–3 km. However, anisotropy appears to be regional as we see similar splitting at both NA and SEA, which are separated by 10 km.

[46] **Acknowledgments.** We thank the numerous people involved in instrument deployment, especially UCSB PBIC. We appreciate the support of IRIS-PASSCAL Instrument Center for the use of instruments. Special acknowledgments to the Marine Corps Air Ground Combat Center (MCAGCC), Twenty-nine Palms, California, for permission to conduct the experiment within the base. We also thank associate editor J. Gomberg and reviewer M. Savage and an anonymous reviewer for their valuable comments on this manuscript. We acknowledge support from NSF Graduate Fellowship for ESC, the Southern California Earthquake Center, and NSF grant EAR-0001132.

References

Aster, R. C., and P. Shearer, Initial shear wave particle motions and stress constraints at the Anza seismic network, *Geophys. J. Int.*, *108*, 740–748, 1992.

Aster, R. C., P. M. Shearer, and J. Berger, Quantitative measurements of shear wave polarizations at the Anza seismic network, southern California: Implications for shear wave splitting and earthquake prediction, *J. Geophys. Res.*, *95*(B8), 12,449–12,473, 1990.

Booth, D. C., and S. Crampin, Shear-wave polarizations on a curved wavefront at an isotropic free surface, *Geophys. J. R. Astron. Soc.*, *83*(1), 31–45, 1985.

Booth, D. C., S. Crampin, and J. H. Lovell, Temporal changes in shear wave splitting during an earthquake swarm in Arkansas, *J. Geophys. Res.*, *95*(B7), 11,151–11,164, 1990.

Crampin, S., Seismic-wave propagation through a cracked solid: Polarization as a possible dilatancy diagnostic, *Geophys. J. R. Astron. Soc.*, *53*(3), 467–496, 1978.

Crampin, S., Geological and industrial implications of extensive-dilatancy anisotropy, *Nature*, *328*, 491–496, 1987.

Crampin, S., The scattering of shear-waves in the crust, *Pure Appl. Geophys.*, *132*(1–2), 67–91, 1990.

Crampin, S., and S. V. Zatsepin, Modelling the compliance of crustal rock—II. Response to temporal changes before earthquakes, *Geophys. J. Int.*, *129*, 495–506, 1997.

Davis, J. C., *Statistics and Data Analysis in Geology*, 646 pp., John Wiley, Hoboken, N. J., 1986.

Fialko, Y., D. Sandwell, D. Agnew, M. Simons, P. Shearer, and B. Minster, Deformation on nearby faults induced by the 1999 Hector Mine earthquake, *Science*, *297*, 1858–1862, 2002.

Gamar, F., and P. Bernard, Shear wave anisotropy in the Erzincan basin and its relationship with crustal strain, *J. Geophys. Res.*, *102*(B9), 20,373–20,393, 1997.

Gao, Y., P. Wang, S. Zheng, M. Wang, Y. Chen, and H. Zhou, Temporal changes in shear-wave splitting at an isolated swarm of small earthquakes in 1992 near Dongfang, Hainan Island, southern China, *Geophys. J. Int.*, *135*, 102–112, 1998.

Hauksson, E., L. M. Jones, and K. Hutton, The 1999 M (sub w) 7. 1 Hector Mine, California, earthquake sequence: Complex conjugate strike-slip faulting, *Bull. Seismol. Soc. Am.*, *92*(4), 1154–1170, 2002.

Hudson, J. A., Wave speeds and attenuation of elastic waves in material containing cracks, *Geophys. J. R. Astron. Soc.*, *64*, 133–150, 1981.

Ji, C., D. J. Wald, and D. V. Helmberger, Source description of the 1999 Hector Mine, California, earthquake, part II: Complexity of slip history, *Bull. Seismol. Soc. Am.*, *92*(4), 1208–1226, 2002.

Leary, P. C., S. Crampin, and T. V. McEvilly, Seismic fracture anisotropy in the Earth's crust: An overview, *J. Geophys. Res.*, *95*(7), 11,105–11,114, 1990.

Li, Y.-G., K. Aki, J. E. Vidale, and F. Xu, Shallow structure of the Landers fault zone from explosion-generated trapped waves, *J. Geophys. Res.*, *104*(B9), 20,257–20,275, 1999.

Li, Y.-G., J. E. Vidale, S. M. Day, and D. D. Oglesby, Study of the 1999 M 7.1 Hector Mine, California, earthquake fault plane by trapped waves, *Bull. Seismol. Soc. Am.*, *92*(4), 1318–1332, 2002.

Mardia, K. V., and P. E. Jupp, *Directional Statistics*, 429 pp., John Wiley, Hoboken, N. J., 2000.

Munson, C. G., C. H. Thurber, Y. Li, and P. G. Okubo, Crustal shear wave anisotropy in southern Hawaii: Spatial and temporal analysis, *J. Geophys. Res.*, *100*(B10), 20,367–20,377, 1995.

Nur, A., and G. Simmons, Stress-induced velocity anisotropy in rock: An experimental study, *J. Geophys. Res.*, *74*(27), 6667–6674, 1969.

Nuttli, O., The effect of the Earth's surface on the S wave particle motion, *Bull. Seismol. Soc. Am.*, *51*(2), 237–246, 1961.

O'Connell, R. J., and B. Budiansky, Seismic velocities in dry and saturated cracked solids, *J. Geophys. Res.*, *79*(35), 5412–5426, 1974.

Savage, M. K., X. R. Shih, R. P. Meyer, and R. C. Aster, Shear-wave anisotropy of active tectonic regions via automated shear-wave polarization analysis, *Tectonophysics*, *165*, 279–292, 1989.

Tadokoro, K., and M. Ando, Evidence for rapid fault healing derived from temporal changes in S wave splitting, *Geophys. Res. Lett.*, *29*(4), 6-1-4, 2002.

Treiman, J. A., K. J. Kendrick, W. A. Bryant, T. K. Rockwell, and S. F. McGill, Primary surface rupture associated with the M (sub w) 7.1 16 October 1999 Hector Mine earthquake, San Bernardino County, California, *Bull. Seismol. Soc. Am.*, *92*(4), 1171–1191, 2002.

Vidale, J. E., and Y. G. Li, Damage to the shallow Landers fault from the nearby Hector Mine earthquake, *Nature*, *421*, 524–525, 2003.

Zatsepin, S. V., and S. Crampin, Modelling the compliance of crustal rock—I. Response of shear-wave splitting to differential stress, *Geophys. J. Int.*, *129*, 477–494, 1997.

Zhang, Z., and S. Y. Schwartz, Seismic anisotropy in the shallow crust of the Loma Prieta segment of the San Andreas fault system, *J. Geophys. Res.*, *99*(B5), 9651–9661, 1994.

Zinke, J. C., and M. D. Zoback, Structure-related and stress-induced shear-wave velocity anisotropy: Observations from microearthquakes near the Calaveras fault in central California, *Bull. Seismol. Soc. Am.*, *90*(5), 1305–1312, 2000.

E. S. Cochran and J. E. Vidale, Earth and Space Sciences Department, University of California, Los Angeles, CA 90095-1567, USA. (cochran@moho.ess.ucla.edu; vidale@moho.ess.ucla.edu)

Y.-G. Li, Department of Earth Sciences, University of Southern California, Los Angeles, CA 90089-0740, USA. (ygli@usc.edu)